Desalination and Water Treatment
www.deswater.com

doi: 10.5004/dwt.2018.22763

127 (2018) 282–296
September

Facile synthesis of Fe-Al bimetallic hydroxides and its application for individual and competitive adsorption of Cr(VI) and As(III)

Yiang Fan[a,b], Yunhai Wu[a,c,*], Haitao Sha[c], Zhengyuan Zhou[b]

[a]*Key Laboratory of Integrated Regulation and Resources Development of Shallow Lakes, Ministry of Education, Hohai University, 1st Xikang Road, Nanjing 210098, China, Tel./Fax: +86-25-83786697; email: hhuhappy@163.com*
[b]*Department of Civil Engineering, The University of Hong Kong, Pokfulam Road, Hong Kong, China*
[c]*College of Environment, Hohai University, 1st Xikang Road, Nanjing 210098, China*

Received 4 February 2018; Accepted 8 July 2018

ABSTRACT

The iron-aluminum (Fe-Al) hydroxides adsorbent with high efficiency for removal Cr(VI) and As(III) was facilely synthesized via coprecipitation method and applied for individual and competitive adsorption. Fe-Al hydroxides were characterized by Brunauer–Emmett–Teller (BET), scanning electron microscope (SEM), energy dispersive spectroscopy (EDS), X-ray diffraction (XRD), Fourier-transform infrared spectroscopy (FTIR) analysis, and X-ray photoelectron spectroscopy (XPS) to reveal the microstructure of adsorbent and adsorption mechanism. A series of batch experiments were conducted with different parameters (pH, adsorbent dosage, and initial concentration) to determine the optimum condition. The maximum capacity of the Fe-Al hydroxides for Cr(VI) was 33.64 mg/g at pH 5.0 using 1.4 g/L adsorbent and 80 mg/L of initial concentration; and As(III) was 8.12 mg/g at pH 6.0 with 1.4 g/L adsorbent and 16 mg/L of initial concentration, respectively. In the single component system, the adsorption of both Cr(VI) and As(III) better fitted with Langmuir isotherm and pseudo-second-order kinetic model. In the binary system, the results showed that the extended Freundlich isotherm model (EFIM) was suitable for evaluating adsorption equilibrium data with reasonable regression coefficients. The desorption studies showed the best recovery of heavy metals in NaOH.

Keywords: Fe-Al hydroxides; Adsorption; Cr(VI); As(III); Binary system

1. Introduction

Water contamination by heavy metals has become a significant issue throughout the world with the rapid industrialization and urbanization. As one of the priority contaminants, Cr(VI) is widely present in effluents drained from industries such as electroplating, leather tanning, pigments, and textile with varied concentrations (5–220 mg/L) in aquatic environment. Due to its high toxicity, carcinogenicity, and mutagenicity [1], US EPA set the maximum level of Cr(VI) in drinking water at 0.05 mg/L [2]. Arsenic (As) is also one of the toxic contaminants that derived from the pathogenic sources occurs in surface soils. Moreover, As(III) redox state is considerably more poisonous and the maximum contaminant level for As(III) in US drinking water is 10 μg/L on the grounds of its high toxicity [3].

In terms of the treatment of Cr(VI) and As(III), various methods have been developed including chemical precipitation, ion exchange, membrane separation, photocatalytic reduction, and adsorption [4,5]. However, none of these methods are ideal, since every method has its disadvantage and limit. Comparing all the advantages and disadvantages of the above-mentioned strategies, adsorption processes are considered as efficient and low-cost means for the removal of heavy metals due to their cost-effectiveness and ease of operation.

Recent years, many researchers have hammered at developing effective adsorbents, such as activated carbon [6], waste agricultural materials [7], carbon–clay nanocomposites [8],

* Corresponding author.

and metal hydroxides [9]. In comparison with other adsorbents, metal hydroxides are more promising on the grounds of their excellent adsorption properties for heavy metals, their common existence in the natural environment and their great possibility to realize engineering application. Among metal hydroxides materials, Fe and Al hydroxides are cheap, eco-friendly and widely used. Albeit Fe or Al hydroxides have great application in water treatment, the utilization of mixed Fe-Al hydroxides is rare. Biswas et al. [10] had applied Fe-Al hydroxides to absorb fluoride from aqueous solutions, thus the Fe-Al hydroxides could be anticipated to be effective in removing other contaminants such as Cr(VI) and As(III).

In this work, the composited Fe-Al hydroxides were successfully synthesized by facile and effective strategy for removing Cr(VI) and As(III) in aqueous solution. The Fe-Al hydroxides were characterized by Brunauer–Emmett–Teller (BET), scanning electron microscope (SEM), energy dispersive spectroscopy (EDS), X-ray diffraction (XRD), Fourier-transform infrared spectroscopy (FTIR) analysis, and X-ray photoelectron spectroscopy (XPS). The effects of pH, adsorbent dosage, and initial concentration of heavy metals were investigated in the single component system to determine the optimum conditions for the adsorption process. Isotherm equilibrium and adsorption kinetics were comprehensively investigated in both single and binary component system to determine the adsorption mechanism.

2. Materials and methods

2.1. Materials

Reagents used in this research were analytically pure and purchased from Sinopharm Chemical Reagent Co., Ltd. (Shanghai Chemical Company, Shanghai, China). The stock solution of 100 mg/L Cr(VI) was prepared by dissolving 0.2829 g $K_2Cr_2O_7$ in 1 L deionized water, a stock solution of 1,000 mg/L As(III) was prepared with deionized water using $NaAsO_2$. pH of the solution was adjusted with 0.1 M of HCl or 0.1 M of NaOH.

2.2. Synthesis and characterization of Fe-Al hydroxides

A modified coprecipitation method [11] was applied for the preparation of Fe-Al hydroxides. In general, 500 mL of 0.1 M $FeCl_3$ (with several drops of 0.01 M HCl) and 500 mL of 0.1M $AlCl_3$ (with several drops of 0.01 M HCl) were mixed together to form a 1 L solution and heated to 338 K. Then, 2.0 M NaOH was dropped into the mixture under vigorous magnetic stirring until the pH of the solution reached about 7.4. After 12 h of aging, the fluffy precipitate was centrifuged at 6,000 rpm for 5 min and the compact precipitate was separated by filtration, washed twice by deionized water and dried at 378 K for 24 h in an oven. Finally, the dried product was ground and sieved to pass 100 mesh by standard sieves as adsorbent and stored in a desiccator for further use.

The Fe-Al hydroxides were characterized by a series of techniques. N_2 adsorption–desorption isotherms were performed at 77 K with ASAP 2010 Surface Analyzer (Micromeritics Instrument Corp., USA). The surface area and pore size of Fe-Al hydroxides were calculated by BET equation and BJH method. The morphology of Fe-Al hydroxides was observed by SEM (SIGMA, Carl Zeiss, Germany) and the elemental composition was analyzed by EDS (SIGMA, Carl Zeiss, Germany). The crystallinity of the sample was investigated by an XRD diffractometer (SRA M18XHF, MAC Science Co. Ltd., Japan). FTIR analysis with KBr disks containing ground samples was performed in an FTIR spectrometer (Spectrum 100, PerkinElmer Corp., USA) and XPS spectra were obtained with an electron spectrometer (ESCALab220iXL, VG Scientific, UK) using 300 W Al Kα radiation.

2.3. Batch adsorption experiments

Adsorption experiments in the single system were carried out in conical flasks with 50 mL of Cr(VI) or As(III) solutions. The conical flasks were shaken at 140 rpm for 4 h. A series of experiments were conducted by varying initial pH (3.0–9.0), adsorbent dosage (0.2–1.6 g/L), and initial metal ion concentrations (10–80 mg/L for Cr(VI), 2–16 mg/L for As(III)) in order to investigate that how these factors affect adsorption performance. The effects of initial pH were conducted with 30 mg/L Cr(VI) or 10 mg/L As(III), the adsorption dosage is 1.0 g/L. In a binary system, the effect of pH on the adsorption of Cr(VI) or As(III) was also investigated in the range of 3.0–9.0. Equilibrium isotherm was determined with different initial concentration of Cr(VI) (10–80 mg/L) and As(III) (2–50 mg/L) at 298, 308, and 318 K. For kinetic studies, samples were withdrawn at predetermined time intervals. After adsorption, the samples were filtered and the residue solutions were examined to determine the concentration by an ultraviolet spectrophotometer (UV-1201, Rayleigh, Beijing, China) at a wavelength of 540 nm for Cr(VI) and 510 nm for As(III), respectively. The standard solutions of Cr(VI) (0.004–0.2 mg/L) and As(III) (0.02–0.5 mg/L) were prepared from stock solutions to plot calibration curves (Fig. S1), and the coefficient (R^2) was 0.9966 and 0.9949 for Cr(VI) and As(III), respectively.

All of the batch experiments were conducted in triplicate and the average value was used for data analysis.

The adsorption efficiency (%) and adsorption capacity (q_e (mg/g)) of heavy metals were depicted as following equations:

$$\text{Sorption}(\%) = \frac{C_0 - C_e}{C_0} \times 100\% \quad (1)$$

$$q_e = \frac{(C_0 - C_e)V}{M} \quad (2)$$

where C_0 is the initial metal concentration (mg/L), C_e is the final metal concentration (mg/L), V (L) is the volume of the solution, and M (g) is mass of the dry adsorbent.

2.4. Desorption experiments

The desorption experiments were carried out by adding 0.1 g of adsorbents loaded with heavy metals in conical flasks with 100 mL of 10 mM eluents. Five types of eluents were used for desorption, including HCl, CH_3COOH, NaCl,

Na_2CO_3, and NaOH. The desorption ratio can be calculated according to the following equation:

$$\text{Desorption ratio}(\%) = \frac{C_2 \times V_2}{(C_0 - C_e) \times V_1} \quad (3)$$

where C_2 is final metal concentration after reaching desorption equilibrium (mg/L) and V_1 (L) and V_2 (L) are volumes of heavy metal solution and eluent, respectively.

Meanwhile, in order to test the regeneration property of Fe-Al hydroxides, the five cycles of adsorption–desorption experiments were also carried out by using the recovered adsorbents for repeated adsorption (50 mg/L of Cr(VI) and 10 mg/L of As(III) under optimum conditions), and the adsorption capacities of Fe-Al hydroxides for Cr(VI) and As(III) in each cycle were recorded.

3. Results and discussion

3.1. Characterization of Fe-Al hydroxides

After completing the synthesis of Fe-Al hydroxides, the surface area and pore size of adsorbent material were analyzed by BET. The BET surface area of Fe-Al hydroxides was 294.979 m^2/g, the measured pore volumes were 0.261 cm^3/g, and the average pore diameter was 3.756 nm. The relatively large surface indicates that the Fe-Al hydroxides could have good adsorption property. The pore size distribution of Fe-Al hydroxides was shown in Fig. S2. After adsorption process, the BET surface area decreased slightly to 289.632 m^2/g, with pore volumes decreasing to 0.248 cm^3/g, which indicated that the heavy metal ions have been adsorbed onto the surface of adsorbents and occupied the binding sites.

The surface morphology and elemental composition of Fe-Al hydroxides before and after adsorption process were studied by SEM and EDS (Fig. 1). It could be distinguished clearly from SEM figures that the original Fe-Al hydroxides (Fig. 1(a1)) have coarse surfaces with small steps, suggesting the existence of gibbsite in Fe-Al hydroxides, which can provide >$AlOH_2$ as binding sites [12]. But the adsorbent surface became smooth after adsorption of Cr(VI) and As(III) (Fig. 1(b1)). Generally speaking, the uneven surface could be helpful for the adsorption of heavy metals, then the holes of adsorbent would be blocked after the adsorption and the surface would be glossy. Fig. 1(a2) revealed that the Fe-Al hydroxides were successfully synthesized, Fig. 1(b2) showed that the Fe-Al hydroxides had adsorbed Cr(VI) and As(III) simultaneously.

In order to test whether the Fe-Al hydroxides was synthesized successfully and observe the diffraction peaks' change of Fe-Al hydroxides after adsorption, XRD was employed to examine samples. X-ray diffraction results (Fig. 2) showed that the synthesized Fe-Al hydroxides have poor crystalline with broad background peaks. Peaks centered at 2θ values of 18.3°, 20.3°, 27.9°, and 37.6° are corresponding to the (002), (110), (112), and (311) planes of gibbsite (JCPDS No. 07–0324), peaks located at 2θ = 35.1° (100), 40.4° (011), 53.8° (012), 62.9° (110), and 87.6° (202) can be well indexed as iron oxide

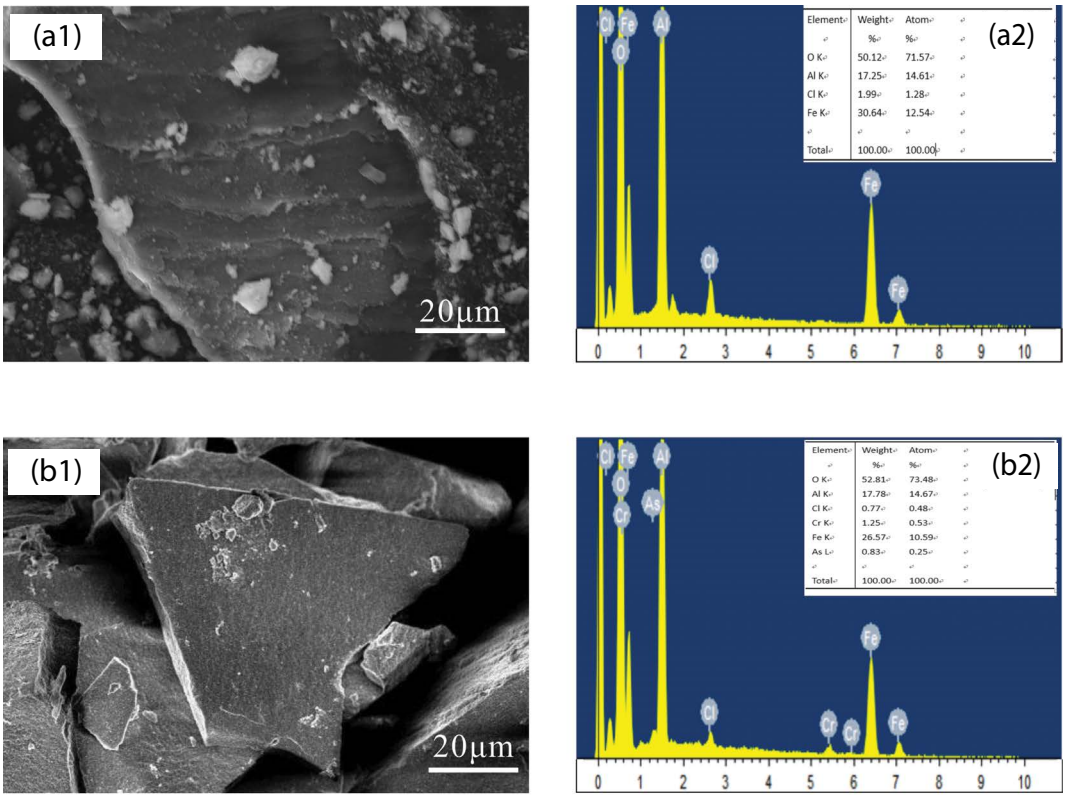

Fig. 1. The SEM and EDS for Fe-Al hydroxides before and after adsorption. (a1, a2): original Fe-Al hydroxides; (b1, b2): Fe-Al hydroxides after adsorbing Cr(VI) and As(III).

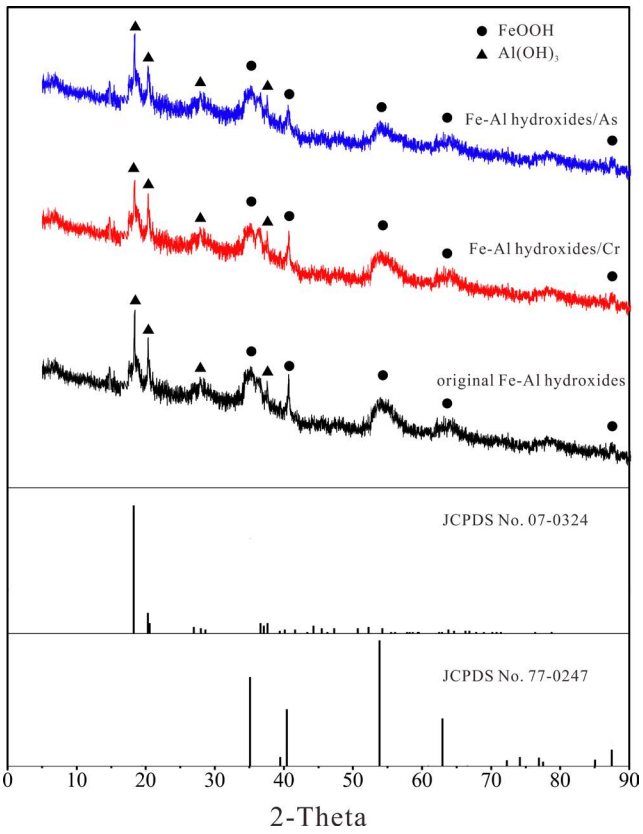

Fig. 2. Powder XRD patterns of Fe-Al hydroxides before and after adsorption.

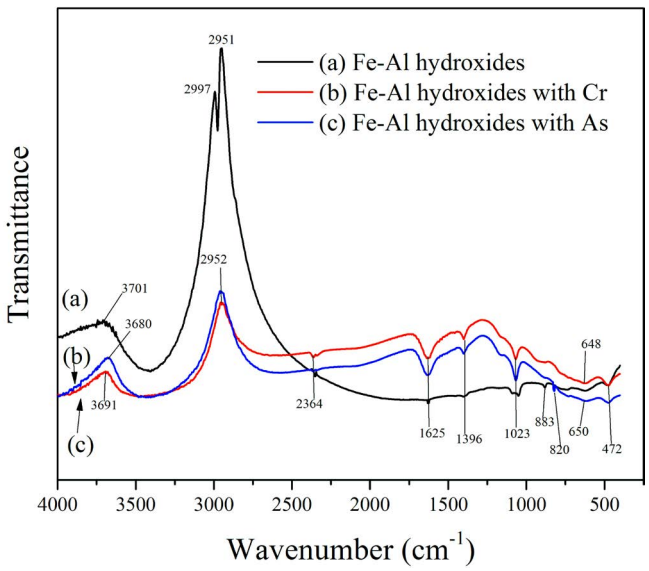

Fig. 3. FTIR spectra of Fe-Al hydroxides before (a) and after adsorption of Cr(VI) (b) and As(III) (c).

hydroxides (JCPDS No. 77–0247). The diffraction patterns of Fe-Al hydroxides with Cr(VI) or As(III) loading are similar to original Fe-Al hydroxides patterns, which means the crystal phase of bimetal hydroxides is stable. But the diffraction peaks of iron oxide hydroxides and gibbsite all weaken to different extents after adsorption process. These phenomena may be due to the lattice strain caused by the differences of various atomic sizes [13].

FTIR spectra of Fe-Al hydroxides before and after adsorption are shown in Fig. 3. The band at 1,625 cm^{-1} was designated to the deformation of water molecules, suggesting that the physisorbed water was presented on the hydroxides [14]. Peaks at 3,680, 3,691, and 3,701 cm^{-1} were assigned to the O–H stretching vibration [15]; the bands at 2,951, 2,952, and 2,997 cm^{-1} were attributed to the broad O–H stretching vibration [16]; peaks at 2,364 cm^{-1} were suggested to the O–H stretching vibration. The occurrence of the peak at 1,396 cm^{-1} after adsorption of Cr(VI) and As(III) may be attributed to the interaction between ferric or aluminum hydroxides in adsorbent and metal ions since this peak did not appear in original Fe-Al hydroxides. The band at 1,023 cm^{-1} was due to asymmetrical vibrations for Al–O–H [17]. After reaction with metal ions, the band at 883 cm^{-1} disappeared, suggesting that the redox reaction between Fe-Al hydroxides and metal ions cause the surface alteration. The new peak at 820 cm^{-1} after As(III) adsorption could be attributed to As–O vibration in As(III) species. Bands in the range of 650 cm^{-1} were attributed to metal-oxygen-metal stretching after adsorption process [18]. The peak at 472 cm^{-1} was the characteristic peaks of Fe–O bond in α-FeOOH and γ-$Al(OH)_3$ [19,20] and thus the adsorbent could be confirmed the hydroxides.

According to some related literature [21,22], the valences of some elements on adsorbent and adsorbate may change during the adsorption process. Hence, the XPS was conducted and the spectra of Fe, Al, Cr, and As are presented in Fig. 4. The spectra of Cr and As occurred on the Fe-Al hydroxides after adsorption, illustrating the Cr and As removal directly. The spectra of Fe 2p in original Fe-Al hydroxides are depicted in Fig. 4(a), the peak at 711.6 eV in high-resolution spectra of Fe $2p_{3/2}$ represented Fe(III) in Fe_3O_4 [23], the peak at 724.7 eV in spectra of Fe $2p_{1/2}$ corresponded to Fe_2O_3. In the high resolution of Al 2p in the original Fe-Al hydroxides (Fig. 4(b)), photoelectron peak at 74.2 eV referred to $Al(OH)_3$ [24]. The binding energy peaks of Fe 2p and Al 2p shifted after reaction with Cr(VI) and As(III), the peaks of Fe 2p and Al 2p moved to lower energy (Figs. 4(c) and (d)), probably implying that –OH bonded to Fe-Al were engaged in adsorption of heavy metals and the Fe-Al oxides with low binding energy were formed after adsorption process [25]. Fig. 4(c) illustrates that for Cr-loaded adsorbent, the binding energy for Fe $2p_{3/2}$ at 709.5 eV corresponded to FeO [26], the binding energy peaks at 711.2 and 722.6 eV were ascribed to Fe(III) in Fe oxides [27]; for As-loaded adsorbent, the binding energy peak at 709.5 eV referred to Fe(II), the peaks at 711.8 and 722.7 eV related to Fe(III). Al 2p XPS spectrum after adsorption (Fig. 4(d)) also changed and the peaks shifted to lower energy which illustrated the Al oxides with low binding energy were formed. Moreover, peaks at 73.4 and 73.6 eV both represented Al(III), there were no Al^0 existed after adsorption. After Cr(VI) adsorption, the high-resolution spectra of Cr $2p_{3/2}$ on Cr-loaded Fe-Al hydroxides are shown in Fig. 4(e). Binding energy 576.1 and 578.1 eV were obtained after XPS-peak-differentiation-imitating analysis of Cr $2p_{3/2}$ and the peak at 576.1 eV corresponded to Cr(III) in Cr_2O_3 [28] yet the peak at 578.1 eV referred to Cr(VI) in CrO_3. The Cr(III)

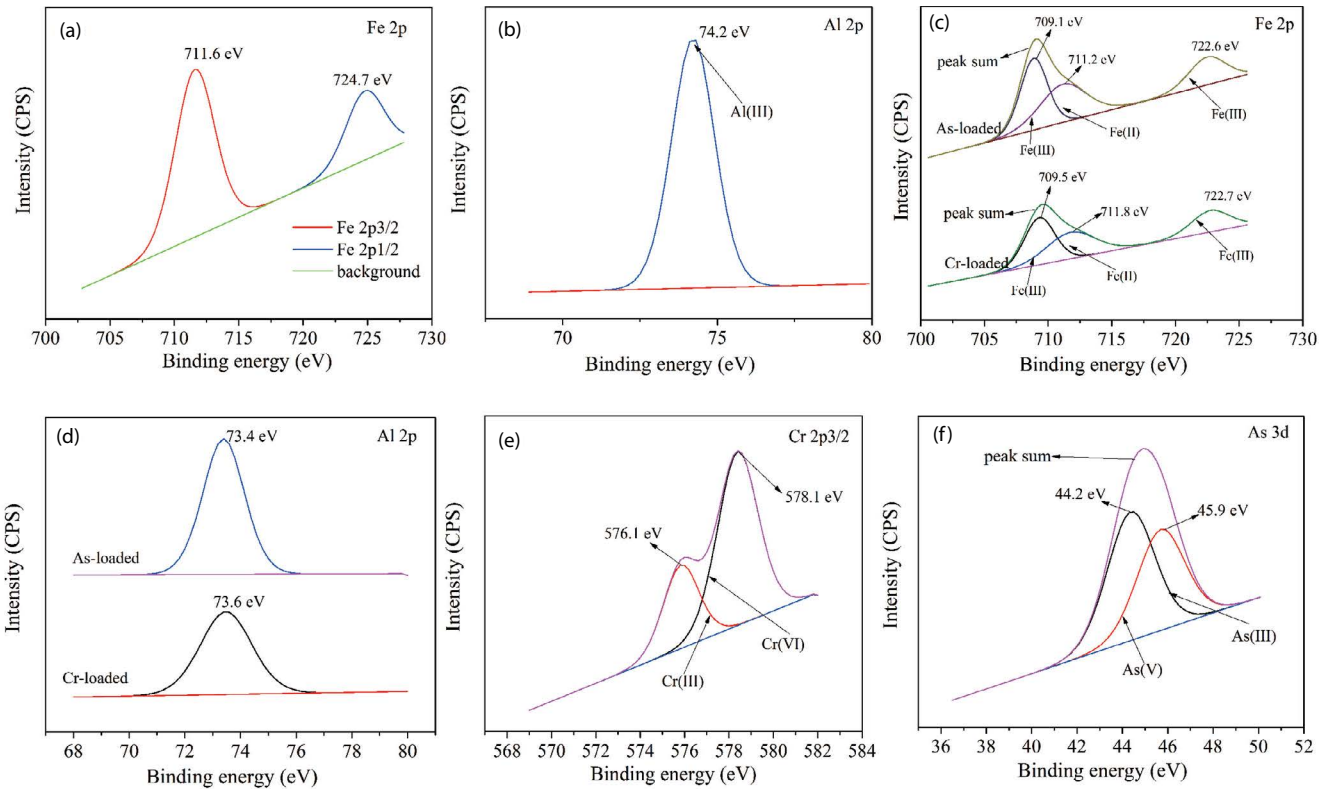

Fig. 4. XPS patterns of (a) Fe 2p of original Fe-Al hydroxides, (b) Al 2p of original Fe-Al hydroxides, (c) Fe 2p of Fe-Al hydroxides after adsorption, (d) Al 2p of Fe-Al hydroxides after adsorption, (e) Cr 2p after adsorption, and (f) As 3d after adsorption.

accounted for 23.57% of Cr(VI) based on peak areas and this result was proved by Wang et al. [25]. Binding energy 44.2 and 45.9 eV for spectra of As 3d are reflected in Fig. 4(f), peak at 44.2 eV represented As(III) in As_2O_3 but peak at 45.9 eV represented As(V) in As_2O_5 [29]. The As(V) occupied 43.98% of As(III) according to peak area analysis and this phenomenon verified that a portion of As valences were raised during the adsorption process and the combination of As(V) with Fe-Al hydroxides was formed. According to the XPS results described previously, the probable mechanism of reaction between Fe-Al hydroxides and heavy metals is depicted in Fig. 5.

Prior to using Fe-Al hydroxides as adsorbents in adsorption process, it is necessary to compare the adsorption performance of Fe-Al hydroxides with that of pure $Fe(OH)_3$ or $Al(OH)_3$, the adsorption experiments using $Fe(OH)_3$, $Al(OH)_3$, and Fe-Al hydroxides were carried out and the results were depicted in Fig. S3. The concentrations of heavy metal ions were 10 mg/L; the adsorption dosage was 1.0 g/L. It can be easily found that the adsorption ratios for Cr(VI) by $Fe(OH)_3$ and $Al(OH)_3$ are 71.23% and 73.62%, respectively, but the removal ratio increases to 89.23% when Fe-Al hydroxides are used as adsorbents for adsorption. The Fe-Al hydroxides can remove 95.37% of As(III) from aqueous solution, while $Fe(OH)_3$ and $Al(OH)_3$ can only remove 86.11% and 69.18% of As(III). From the XRD analysis of Fe-Al hydroxides and other researchers' previous work [30], the Al^{3+} was largely incorporated into the structure of iron oxide hydroxides, leading to the lattice expansion and the formation of microcrystal structure in Fe-Al hydroxides [31], which will result in the improvement of adsorption capability [32]. Moreover, the Fe-Al hydroxides can provide more binding sites for heavy metal ions, hence the bimetallic hydroxides exhibit significantly high adsorption performance compared with that of single metal hydroxide. In addition, considering the better adsorption performance of bimetallic hydroxides, there is no need to use single metal hydroxide as a comparison in following adsorption experiments.

3.2. Single component system adsorption experiment

3.2.1. Effect of initial pH

The process of adsorption depends mainly on solution pH values, which affect both the ionization degree and surface property of the adsorbents. The effect of pH on Cr(VI) or As(III) adsorption is shown in Fig. 6(a), which illustrates that the maximum adsorption capacity of Cr(VI) (26.35 mg/g) is observed at pH 5.0 and the maximum adsorption capacity of As(III) (8.34 mg/g) is observed at pH 6.0. For Cr(VI), the adsorption capacity increased slowly when pH range from 3.0 to 5.0 and decreased gently from pH 5.0 to pH 6.0, but decreased sharply after pH 6.0. This suggests that the adsorption of Cr(VI) onto Fe-Al hydroxides has a wide suitable pH range. For As(III), the adsorption capacity increased greatly before pH 6.0 but decreased after pH 6.0.

The distribution of Cr(VI) (Fig. S4(a)) and As(III) (Fig. S4(b)) as functions of pH was obtained with the help of Visual MINTEQ [33] and Excel. According to Fig. S4(a), when pH < 5.0, the dominant form of Cr(VI) was $HCrO_4^-$ and

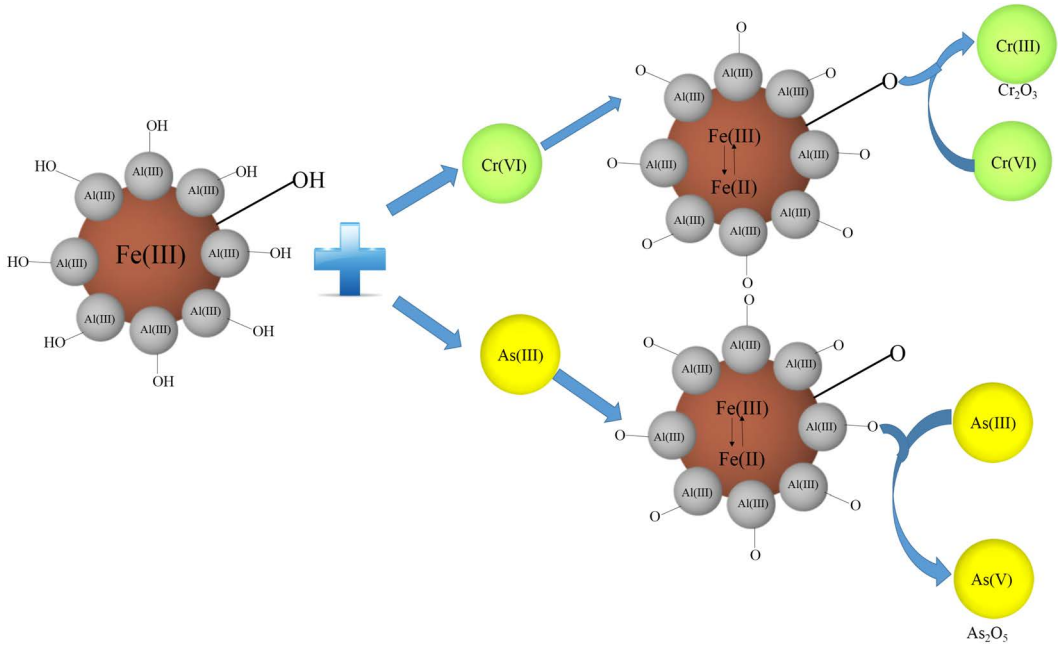

Fig. 5. The reaction mechanism between Fe-Al hydroxides and Cr(VI)/As(III) during the adsorption process.

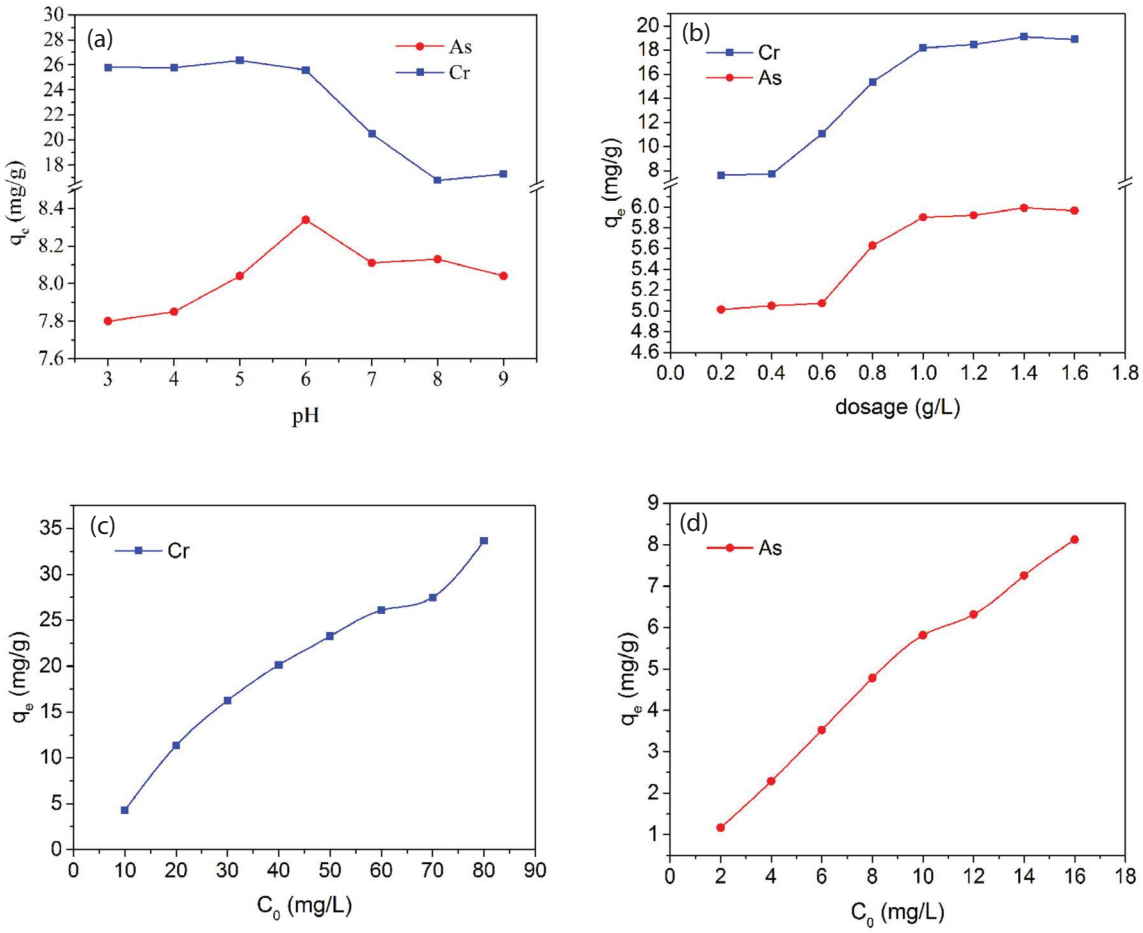

Fig. 6. Effect of initial pH (a), adsorbent dosage (b), initial Cr(VI) concentration (c) and initial As(III) concentration (d) on adsorption of Cr(VI) and As(III) on Fe-Al hydroxides.

other researchers also had this conclusion [34]. In an acidic environment, the –OH on the Fe-Al hydroxides were easily protonated. The mechanism for pH-dependent interaction of Cr(VI) on Fe-Al hydroxides could be represented as follows [10]:

$$\equiv M-OH + H^+ \leftrightarrow \equiv M-OH_2^+ \quad (4)$$

$$\equiv M-OH_2^+ + HCrO_4^- \leftrightarrow \equiv M-HCrO_4^- + H_2O \quad (5)$$

where M represents metal ions (Fe or Al), M–OH stands for the Fe-Al hydroxides, M–OH_2^+ represents Fe-Al hydroxides with protonated surface hydroxyl groups, and M–$HCrO_4^-$ a surface site occupied by $HCrO_4^-$.

These two steps were favorable at lower pH, while at pH > 6.0, the Cr(VI) ions were predominantly adsorbed by the following process:

$$\equiv M-OH + HCrO_4^- \leftrightarrow \equiv M-HCrO_4^- + HO^- \quad (6)$$

The higher adsorption of Cr(VI) at low pH could be attributed to the positive surface of Fe-Al hydroxides which leads to prominent increase of Cr(VI) adsorption through electrostatic interaction between positively charged metal hydroxides' surface and negatively charged Cr(VI) ions as described in Eqs. (4) and (5). As the solution pH continued increasing, the positively charged sites on Fe-Al hydroxides decreased, and the electrostatic repulsion between Cr(VI) and adsorbent became elevated. Besides, the ligand exchange interaction between Cr(VI) and adsorbent occurred at neutral and alkaline pH region as Eq. (6) depicts. Competition of OH^- for limited adsorption sites became more severe with the increasing pH.

As demonstrated in Fig. S4(b), the dominant species of As(III) before pH 7.0 were H_3AsO_4 and there was no electronic attraction between H_3AsO_4 and adsorbent. Thus, the adsorption of As(III) may be attributed to van der Waals force between the adsorbent surface and adsorbate [33]. When pH was higher than 7.0, the $H_2AsO_3^-$ gradually become dominant species, the electronic repulsion between As(III) and adsorbent could reduce the adsorption of As(III), and the competition of OH^- for active sites on Fe-Al hydroxides could also cause the decrease for As(III) adsorption [17].

3.2.2. Effect of adsorbent dosage

The dosage study is significant due to the fact that it could reflect the adsorbability of adsorbent when the initial concentration of metal ions was given. As showed in Fig. 5(b), the adsorption capacity of Cr(VI) or As(III) increased with the increase of adsorbent dosage until 1.4 g/L, then the adsorption capacity remained almost constant with the enhancement of adsorbent dosage. This phenomenon could be attributed to the increased binding sites with a spectrum of binding energy on the surface of Fe-Al hydroxides and therefore the removal efficiency raised gradually [35]. The maximum adsorption capacity (19.11 mg/g adsorbent for Cr(VI) and 5.99 mg/g adsorbent for As(III)) was found at 1.4 g/L because the saturation capacity was reached. Thus, the optimum adsorbent dosage was selected as 1.4 g/L for other batch experiments.

3.2.3. Effect of initial metal ion concentration

The effects of initial concentration on the removal of Cr(VI) or As(III) were studied at optimum pH (pH 5.0 for Cr(VI) and pH 6.0 for As(III)). As shown in Figs. 6(c) and (d), the uptake of metal ions onto Fe-Al hydroxides increased from 4.28 to 33.64 mg/g with the Cr(VI) concentration in the range of 10–80 mg/L, from 1.16 to 8.12 mg/g with the As(III) concentration ranging from 2 to 16 mg/L, respectively. Different metal ions concentrations were selected according to various concentrations of Cr(VI) and As(III) in industrial wastewater.

The initial concentration of metal ions plays a significant role due to the driving force it provides which could overcome mass transfer resistance between the aqueous solution and solid adsorbent during the adsorption process [36]. In fact, as the metal ions concentration raised, the driving force became stronger as well, the accessibility of metal ions to the binding sites on Fe-Al hydroxides was relatively high, ions exchanged frequently, and the uptake of metal ions became more and more [37].

3.2.4. Isotherm analysis

The equilibrium isotherm experiments were conducted for assessment of adsorbent and could provide fundamental data for adsorption process. The adsorption isotherm could be expressed mathematically and the experimental data were often fitted to Langmuir [38] and Freundlich [39] model. The Langmuir model is effective in monolayer adsorption on surfaces and the Freundlich model is valid for nonideal multilayer adsorption [40]. These two models could be expressed by the following equation:

$$\text{Lamgmuir}: q_e = \frac{q_m b C_e}{1 + bc_e} \quad (7)$$

$$\text{Freundlich}: q_e = K_f C_e^n \quad (8)$$

where q_e (mg/g) is the amount of uptake at equilibrium time, q_m (mg/g) is the quantity of metal ions adsorbed at saturation or monolayer adsorption capacity, b is the equilibrium constant, and K_f and n are constants related to adsorption.

As shown in Figs. 7(a1) and (a2) and Table 1, the Cr(VI) adsorption data fitted to Langmuir and Freundlich models very well, the regression coefficient (R^2) exceeded 0.90 for both models, but the Langmuir could better describe the adsorption process with higher R^2 value, suggesting that the adsorption of Cr(VI) onto Fe-Al hydroxides to be monolayer. Figs. 7(b1) and (b2) depicted the fitting result of As(III) adsorption data for two models, suggesting that the adsorption process of As(III) fitted very well to both Langmuir model and Freundlich model. The value of R^2 in Table 1 could reveal that the adsorption data could be better described by Langmuir model with higher R^2. The values of b in Langmuir model were between 0 and 1 for both Cr(VI) and As(III), which illustrated that the isotherm is favorable.

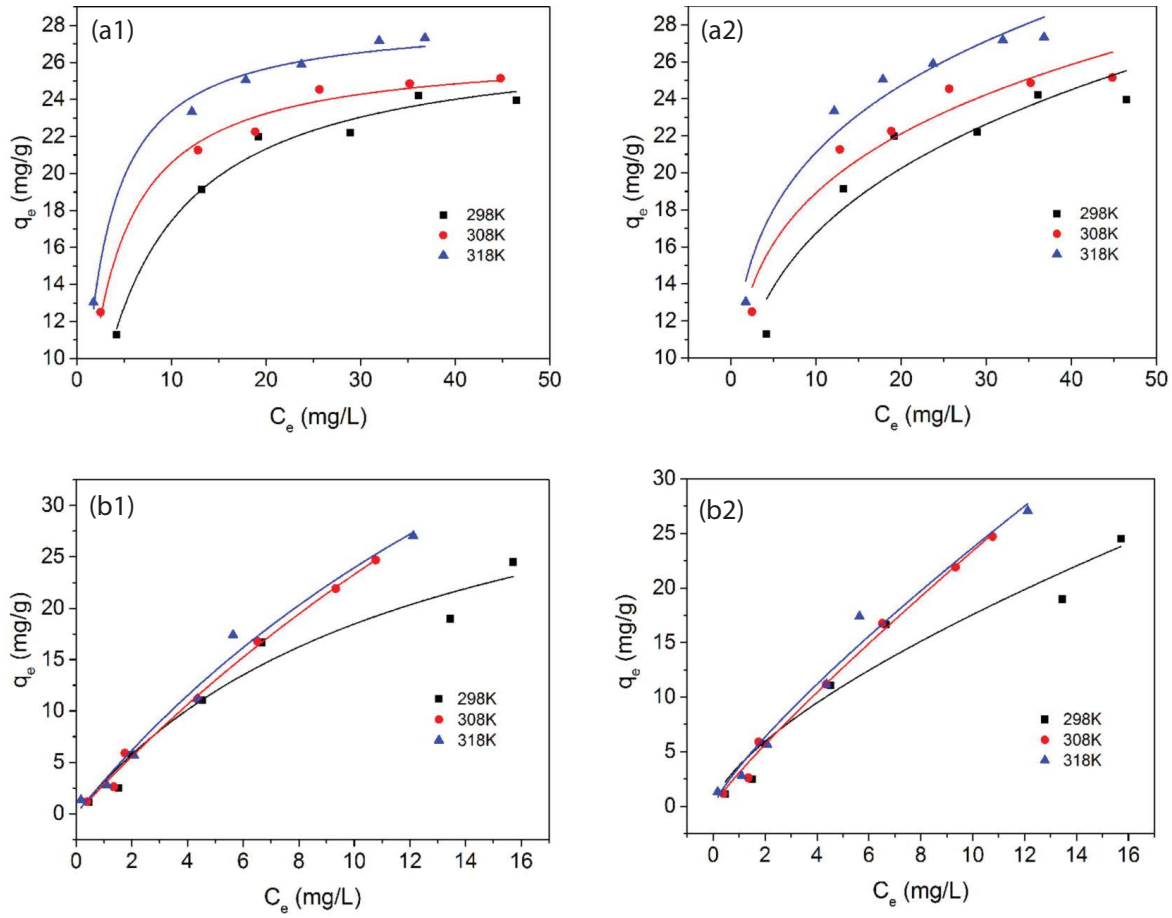

Fig. 7. Adsorption isotherm models for Cr(VI) (a1, a2) and As(III) (b1, b2). (a1, b1): Langmuir isotherm model; (a2, b2): Freundlich isotherm model.

Table 1
Adsorption isotherm constants for the adsorption of As(III) and Ni(II) by the Fe-Al hydroxides in single system

Model	Parameters	Cr(VI)			As(III)		
		298 K	308 K	318 K	298 K	313 K	328 K
Langmuir	q_m (mg/g)	28.4541	26.6877	27.4567	41.0793	113.7960	85.7407
	b (L/mg)	0.4593	0.3368	0.1741	0.0816	0.0257	0.0387
	R^2	0.9881	0.9853	0.9807	0.9562	0.9937	0.9813
Freundlich	n	3.6382	4.4335	4.3760	1.4861	1.1350	1.2217
	K_F (mg/g)	8.8856	11.2501	12.4667	3.7299	3.0750	3.5971
	R^2	0.8798	0.9254	0.9556	0.9365	0.9923	0.9743

3.2.5. Kinetic study

Kinetic studies were often conducted to evaluate the uptake rate and the mechanism of adsorption. In this investigation, the kinetic parameters were analyzed by plotting the adsorption efficiency of heavy metal ions for different agitation times at a constant initial concentration and temperature. Figs. S4(a) and (b) displayed the effect of sorption time on removal efficiency of Cr(VI) and As(III) from the single system. The pseudo-first-order [41] and pseudo-second-order models [42] were applied to evaluate the kinetic data and the results are shown in Table 2. The pseudo-first-order model was applied to depict the adsorption of liquid/solid system based on solid capacity [43], which can be expressed as follows:

$$q_t = q_e\left(1 - e^{-K_1 t}\right) \tag{9}$$

where q_t (mg/g) is metal uptake at time t (min) and K_1 (min^{-1}) is rate constant of pseudo-first-order equation.

Table 2
Kinetic parameters for Cr(VI) and As(III) adsorption in single system

Metal ion	Pseudo-first-order			Pseudo-second-order		
	k_1 (min^{-1})	q_e (mg/g)	R^2	h (mg g^{-1} min^{-1})	q_e (mg/g)	R^2
Cr(VI)	0.0230	14.6896	0.9387	0.5346	16.3496	0.9977
As(III)	0.0869	6.0326	0.8175	0.9042	6.3533	0.9878

The pseudo-second-order model was used for analyzing the adsorption mechanism of rate-controlling steps [44], which can be depicted by the following equations:

$$q_t = \frac{q_e^2 K_2 t}{1 + q_e K_2 t} \tag{10}$$

$$h = K_2 q_e^2 \tag{11}$$

where K_2 (g mg^{-1} min^{-1}) is the rate constant of pseudo-second-order model and h (mg g^{-1} min^{-1}) is the initial reaction rate.

As shown in Figs. S5(a) and (b), the pseudo-second-order model gave an excellent adaption to the adsorption data. The values of R^2 in pseudo-second-order model (0.9977 for Cr(VI), 0.9878 for As(III)) are higher than that of pseudo-first-order model (0.9387 for Cr(VI), 0.8175 for As(III)), which suggest that the pseudo-second-order model is more applicable and the adsorption process is chemisorption process involving sharing or exchange of electrons between metal ions and –OH on Fe-Al hydroxides [45]. A comparison of adsorption capacity for Cr(VI) and As(III) by Fe-Al hydroxides and other reported adsorbents was made as presented in Table 3. It is obvious in Table 3 that the fabricated Fe-Al hydroxides show a better adsorption performance than previous work.

3.3. Binary component system adsorption experiment

3.3.1. Effect of pH

The adsorption efficiency of Cr(VI) and As(III) versus pH in the binary system was shown in Fig. S6. As can be seen in Fig. S6, the results of Cr(VI) and As(III) adsorption in a binary component system exhibited a similar trend to that of a single system. Whereas, both Cr(VI) and As(III) adsorption efficiency decreased in a binary system when compared with that in a single system, which illustrated that the existence of As(III) or Cr(VI) inhibited the adsorption process of Cr(VI) or As(III). When the amount of adsorbent was fixed, the coexisted metal ions would compete for limited adsorption sites on the adsorbent and thus the adsorption results for one of the metal ions would descend. Meanwhile, the adsorption capacity for Cr(VI) and As(III) in binary system was also studied and the results are shown in Fig. S7. In binary system, 100 mL of 0.5 mM Cr(VI) and 100 mL of 0.5 mM As(III) were mixed together to make sure the system has the equal amounts of Cr(VI) and As(III) ions. Fig. S7 illustrated that the adsorption capacity for Cr(VI) decreased from 16.23 to 14.73 mg/g, and the adsorption capacity for As(III) reduced from 12.47 to 7.19 mg/g, when compared with that in single system. The Fe-Al hydroxides in binary system have much higher adsorption capacity for Cr(VI) than for As(III), even though the amounts of Cr(VI) and As(III) ions are equal. This is because that both electrostatic attraction and ligand exchange interaction between Cr(VI) and adsorbents contribute to the adsorption of Cr(VI), while only van der Waals force (relatively weak) between As(III) and adsorbents accounts for the adsorption of As(III), which make Cr(VI) ions have more opportunity to occupy the adsorption sites on Fe-Al hydroxides than As(III).

3.3.2 Binary component system isotherm studies

Albeit the Langmuir and Freundlich isotherm could well depict the adsorption process in the single component system, they could not describe the relationship between adsorbent and adsorbate in the binary or multicomponent system. Accordingly, the extended Langmuir isotherm model (ELIM)

Table 3
Adsorption capacity of MGTW and other reported adsorbents

Adsorbent	Adsorption capacity (mg/g)		C_0 (mg/L)	References
	For Cr(VI)	For As(III)		
Peanut shell derived carbon	6.25	–	50	[46]
Phosphoric acid activated peanut shell	27.64	–	100	[47]
Chitosan based nanohydrogel	25.00	–	120	[48]
Fe-Al hydroxides	33.64	–	80	Present study
Modified green tea waste	–	0.2096	23	[49]
Activated *Moringa oleifera*	–	7.375	20	[50]
Nanofibers of resorcinol–formaldehyde	–	11.09	1,000	[51]
Fe-Al hydroxides	–	8.12	16	Present study

[52] and extended Freundlich isotherm model (EFIM) [53] were selected to reveal the adsorption progress in Cr(VI) and As(III) binary component system. The ELIM assumes a homogeneous surface with respect to the energy of adsorption, no interaction between adsorbed species and all binding sites are equally available to adsorbates. The equation of ELIM is depicted as follows:

$$q_i = \frac{q_{\max} K_i C_{e,i}}{1 + \sum_{J=1}^{N} K_j C_{e,j}} \tag{12}$$

where q_i is the amount of metal i adsorbed per mass of adsorbent, mg/g; $q_{\max}$ is the maximum adsorption capacity of metal i, mg/g; K_i and K_j are the ELIM constant of metal i and j, respectively; and $C_{e,i}$ and $C_{e,j}$ (mg/L) are the concentration of metal i and j in aqueous solution at equilibrium, respectively.

The EFIM is an empirical formula describing adsorption onto a heterogeneous surface. The EFIM is commonly presented as:

$$q_1 = \frac{k_{f,1} C_{e,1}^{\frac{1}{n_1}+x_1}}{C_{e,1}^{x_1} + y_1 C_{e,2}^{z_1}} \tag{13}$$

$$q_2 = \frac{k_{f,2} C_{e,2}^{\frac{1}{n_2}+x_2}}{C_{e,2}^{x_2} + y_2 C_{e,1}^{z_2}} \tag{14}$$

where $C_{e,1}$ is the concentration of metal 1 in aqueous solution at equilibrium and $C_{e,2}$ is the concentration of metal 2 in aqueous solution at equilibrium, mg/L; $k_{f,1}$ and $k_{f,2}$ are the EFIM equilibrium constants of metal 1 and 2, respectively; and n_1, n_2, x_1, x_2, y_1, y_2, z_1, and z_2 are the EFMI constants.

For this paper, in one of the binary adsorption experiments, the Cr(VI) concentration remains 30 mg/L (0.6 mM), and the concentration of As(III) ranges from 7.5 to 75 mg/L (0.1–1.0 mM); in the other experiment, the As(III) keep the concentration at 45 mg/L (0.6 mM) and the concentration of Cr(VI) are in the range of 5–50 mg/L (0.1–1.0 mM). The data obtained in experiments were selected to fit the ELIM and EFIM and the equilibrium concentrations of As(III) or Cr(VI) are plotted to the uptake of Cr(VI) or As(III) in Fig. 8. The parameter values of two models were shown in Table 4. As can be observed in Fig. 8, the adsorption equilibrium data of Cr(VI) in binary system fell over the surface of EFIM and the R^2 value is 0.9895. The fit result of As(III) shows that the EFIM is more suitable.

3.4. Desorption and regeneration studies

After adsorption process, it is necessary to recover heavy metals by desorption, and adsorbents should be reused for repeated adsorption–desorption cycles. Here we use five types of eluents for desorption, and the results were illustrated in Fig. S8. As can be seen in Fig. S8, Na_2CO_3 and NaOH can be regarded as effective eluents for both Cr(VI) loaded adsorbents and As(III) loaded adsorbents, due to their higher desorption ratios than other three types of eluents. Since Na_2CO_3 and NaOH can provide basic condition for adsorbents, and the heavy metal ions can hardly occupy the binding sites on adsorbents under alkaline condition due to the electronic repulsion and the competition of anion ions such as CO_3^{2-} and OH^-, which have been fully discussed in Section 3.2.1. The acid condition would favor the adsorption of heavy metals mainly due to the electronic attraction, thus the HCl and CH_3COOH nearly have no effects on desorption process. Under neutral condition (NaCl), the ligand exchange between

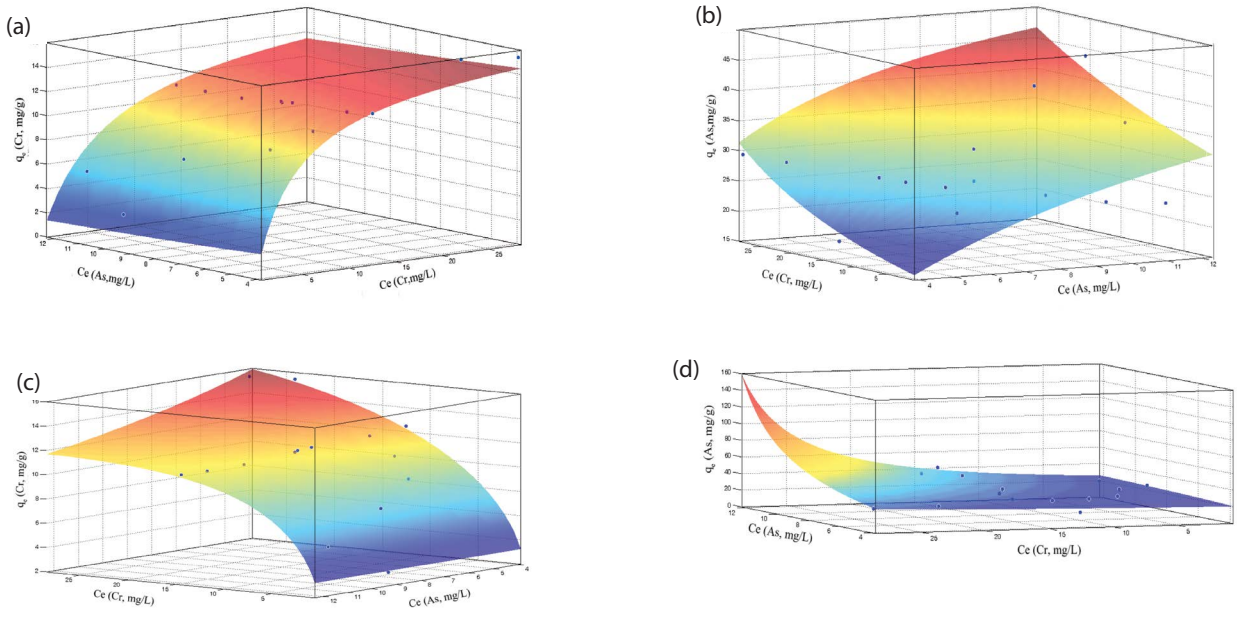

Fig. 8. ELIM for Cr(VI) (a)/As(III) (b) and EFIM for Cr(VI) (c)/As(III) (d) in binary system.

Table 4
Parameters of the ELIM and EFIM models for the binary adsorption of Cr(VI) and As(III) by the Fe-Al hydroxides

Metal ion	ELIM			EFIM					
	K_1	K_2	R^2	$k_{f,i}$	n_i	x_i	y_i	z_i	R^2
Cr(VI)	0.3307	0.09986	0.9200	4.084	2.12	–1.092	0.00186	0.903	0.9895
As(III)	0.0913	–0.02376	0.4682	16.04	5.116	–0.9182	–0.00123	1.26	0.5783

heavy metal ions and Cl^- would be helpful to desorption, so NaCl has a little better effect on desorption process.

As for adsorption–desorption cycles, Fig. S9 shows that the Fe-Al hydroxides have favorable reusability even after five cycles. The NaOH treated adsorbents can still have relatively high adsorption capacities: around 20 mg/g for Cr(VI) and around 4 mg/g for As(III), which are very closed to original adsorbents according to Fig. 6 (23.25 mg/g for Cr(VI) and 5.81 mg/g for As(III)). The decrease in efficiency can be attributed to the inevitable mass loss during repeated adsorption–desorption cycles [54]. So NaOH can be selected as effective eluent for desorption, and the great regeneration property of Fe-Al hydroxides suggested that it can be regarded as cost-effective adsorbents for Cr(VI) and As(III) removal.

4. Conclusion

The composited Fe-Al hydroxides were successfully synthesized and applied in treating wastewater, which contains Cr(VI) and As(III). The BET analysis disclosed that the Fe-Al hydroxides have a relatively high surface area at 294.979 m^2/g. The SEM and EDS analysis revealed that the Fe-Al hydroxides could adsorb heavy metals and the surface of adsorbent would be smoother after adsorption process. The XRD patterns and FTIR analysis showed the existence of iron and aluminum hydroxides in the Fe-Al hydroxides. The XPS assessment revealed that valences of elements involved in adsorption have changed during the adsorption process. It was found that the adsorption capacity reach the maximum (33.64 mg/g for Cr(VI), 8.12 for As(III)) at pH 5.0 (for Cr(VI)) or pH 6.0 (for As(III)), adsorbent dosage of 1.4 g/L and initial concentration of 80 mg/L (Cr(VI)) or 16 mg/L (As(III)) in single component system. The Langmuir isotherm model and pseudo-second-order kinetic model could better fit the adsorption data of both Cr(VI) and As(III) in the single component system. In the binary component system, the EFIM was more suitable for both Cr(VI) and As(III) adsorption equilibrium. NaOH is effective for desorption and alkali treated adsorbents showed good adsorption performance in repeated adsorption–desorption cycles.

Acknowledgment

This work was supported by a project funded by the Priority Academic Program Development of Jiangsu Higher Education Institutions.

References

[1] C.M. Thompson, R.R. Young, M. Suh, H.R. Dinesdurage, R.H. Elbekai, M.A. Harris, A.C. Rohr, D.M. Proctor, Assessment of the mutagenic potential of Cr (VI) in the oral mucosa of Big Blue® transgenic F344 rats, Environ. Mol. Mutagen., 56 (2015) 621–628.
[2] M. Kobya, Adsorption, kinetic and equilibrium studies of Cr (VI) by hazelnut shell activated carbon, Adsorpt. Sci. Technol., 22 (2004) 51–64.
[3] L. Wang, D.E. Giammar, Effects of pH, dissolved oxygen, and aqueous ferrous iron on the adsorption of arsenic to lepidocrocite, J. Colloid Interface Sci., 448 (2015) 331–338.
[4] M. Danish, R. Hashim, M.N.M. Ibrahim, M. Rafatullah, O. Sulaiman, Surface characterization and comparative adsorption properties of Cr(VI) on pyrolysed adsorbents of Acacia mangium wood and *Phoenix dactylifera* L. stone carbon, J. Anal. Appl. Pyrolysis, 97 (2012) 19–28.
[5] Q. Liu, C. Zeng, L. Ai, Z. Hao, J. Jiang, Boosting visible light photoreactivity of photoactive metal-organic framework: designed plasmonic Z-scheme Ag/AgCl@MIL-53-Fe, Appl. Catal., B, 224 (2018) 38–45.
[6] M. Danish, W.A. Khanday, R. Hashim, N.S.B. Sulaiman, M.N. Akhtar, M. Nizami, Application of optimized large surface area date stone (*Phoenix dactylifera*) activated carbon for rhodamin B removal from aqueous solution: Box-Behnken design approach, Ecotoxicol. Environ. Saf., 139 (2017) 280–290.
[7] Y. Wu, Y. Fan, M. Zhang, Z. Ming, S. Yang, A. Arkin, P. Fang, Functionalized agricultural biomass as a low-cost adsorbent: utilization of rice straw incorporated with amine groups for the adsorption of Cr (VI) and Ni (II) from single and binary systems, Biochem. Eng. J., 105 (2016) 27–35.
[8] L. Ai, L. Li, Efficient removal of organic dyes from aqueous solution with ecofriendly biomass-derived carbon@montmorillonite nanocomposites by one-step hydrothermal process, Chem. Eng. J., 223 (2013) 688–695.
[9] L. Ai, C. Zhang, L. Meng, Adsorption of methyl orange from aqueous solution on hydrothermal synthesized Mg–Al layered double hydroxide, J. Chem. Eng. Data, 56 (2011) 4217–4225.
[10] K. Biswas, S.K. Saha, U.C. Ghosh, Adsorption of fluoride from aqueous solution by a synthetic iron (III)-aluminum (III) mixed oxide, Ind. Eng. Chem. Res., 46 (2007) 5346–5356.
[11] X.-H. Wang, F.-F. Liu, L. Lu, S. Yang, Y. Zhao, L.-B. Sun, S.-G. Wang, Individual and competitive adsorption of Cr (VI) and phosphate onto synthetic Fe–Al hydroxides, Colloids Surf. Physicochem. Eng. Aspects, 423 (2013) 42–49.
[12] T. Xu, J.G. Catalano, Impacts of surface site coordination on arsenate adsorption: macroscopic uptake and binding mechanisms on aluminum hydroxide surfaces, Langmuir, 32 (2016) 13261–13269.
[13] F. Fu, Z. Cheng, D.D. Dionysiou, B. Tang, Fe/Al bimetallic particles for the fast and highly efficient removal of Cr (VI) over a wide pH range: performance and mechanism, J. Hazard. Mater., 298 (2015) 261–269.
[14] A.A. Alqadami, M. Naushad, Z.A. Alothman, A.A. Ghfar, Novel metal–organic framework (MOF) Based composite material for the sequestration of U(VI) and Th(IV) metal ions from aqueous environment, ACS Appl. Mater. Interfaces, 9 (2017) 36026–36037.
[15] A.A. Alqadami, M. Naushad, M.A. Abdalla, M.R. Khan, Z.A. Alothman, Adsorptive removal of toxic dye using Fe_3O_4–TSC nanocomposite: equilibrium, kinetic, and thermodynamic studies, J. Chem. Eng. Data, 61 (2016) 3806–3813.
[16] A.A. Alqadami, M. Naushad, M.A. Abdalla, T. Ahamad, Z.A. Alothman, S.M. Alshehri, A.A. Ghfar, Efficient removal of toxic metal ions from wastewater using a recyclable

nanocomposite: a study of adsorption parameters and interaction mechanism, J. Cleaner Prod., 156 (2017) 426–436.
[17] C. Han, L. Zhang, H. Chen, X. Shan, X. Li, W. Zhu, Y. Luo, Removal As (V) by sulfated mesoporous Fe–Al bimetallic adsorbent: adsorption performance and uptake mechanism, J. Environ. Chem. Eng., 4 (2016) 711–718.
[18] I. Ahmed, M. Gasser, Adsorption study of anionic reactive dye from aqueous solution to Mg–Fe–CO_3 layered double hydroxide (LDH), Appl. Surf. Sci., 259 (2012) 650–656.
[19] W. Peng, G. Liu, Infrared Spectra of Minerals, Science Press, Beijing, China, 1982.
[20] M. Naushad, T. Ahamad, B.M. Al-Maswari, A. Abdullah Alqadami, S.M. Alshehri, Nickel ferrite bearing nitrogen-doped mesoporous carbon as efficient adsorbent for the removal of highly toxic metal ion from aqueous medium, Chem. Eng. J., 330 (2017) 1351–1360.
[21] Z. Yu, L. Zhou, Y. Huang, Z. Song, W. Qiu, Effects of a manganese oxide-modified biochar composite on adsorption of arsenic in red soil, J. Environ. Manage., 163 (2015) 155–162.
[22] M. Gheju, I. Balcu, G. Mosoarca, Removal of Cr (VI) from aqueous solutions by adsorption on MnO_2, J. Hazard. Mater., 310 (2016) 270–277.
[23] X. Yin, W. Liu, J. Ni, Removal of coexisting Cr(VI) and 4-chlorophenol through reduction and Fenton reaction in a single system, Chem. Eng. J., 248 (2014) 89–97.
[24] T. Chen, Z. Wu, M. Niu, Y. Xie, X. Wang, Effect of Si–Al molar ratio on microstructure and mechanical properties of ultra-low density fiberboard, Eur. J. Wood Wood Prod., 74 (2015) 1–10.
[25] Y. Wang, D. Liu, J. Lu, J. Huang, Enhanced adsorption of hexavalent chromium from aqueous solutions on facilely synthesized mesoporous iron–zirconium bimetal oxide, Colloids Surf. Physicochem. Eng. Aspects, 481 (2015) 133–142.
[26] N. Ji, X. Wang, C. Weidenthaler, B. Spliethoff, R. Rinaldi, Iron (II) disulfides as precursors of highly selective catalysts for hydrodeoxygenation of dibenzyl ether into toluene, ChemCatChem, 7 (2015) 960–966.
[27] L. Wu, T. Wu, M. Mao, M. Zhang, T. Wang, Electrospinning synthesis of Ni°, Fe° codoped ultrafine-$ZnFe_2O_4$/C nanofibers and their properties for lithium ion storage, Electrochim. Acta, 194 (2016) 357–366.
[28] S.R. Chowdhury, E.K. Yanful, A.R. Pratt, Chemical states in XPS and Raman analysis during removal of Cr (VI) from contaminated water by mixed maghemite–magnetite nanoparticles, J. Hazard. Mater., 235 (2012) 246–256.
[29] C. Wagner, D. Briggs, M. Seah, Practical surface analysis, Auger X-ray Photoelectron. Spectrosc., 1 (1990) 595.
[30] Y. Masue, R.H. Loeppert, T.A. Kramer, Arsenate and arsenite adsorption and desorption behavior on coprecipitated aluminum: iron hydroxides, Environ. Sci. Technol., 41 (2007) 837–842.
[31] P. Sudarsanam, B. Hillary, D.K. Deepa, M.H. Amin, B. Mallesham, B.M. Reddy, S.K. Bhargava, Highly efficient cerium dioxide nanocube-based catalysts for low temperature diesel soot oxidation: the cooperative effect of cerium- and cobalt-oxides, Catal. Sci. Technol., 5 (2015) 3496–3500.
[32] D. Wang, J. Zhang, L. Guo, X. Dong, H. Shen, F. Fu, Synthesis of nano-porous Bi_2WO_6 hierarchical microcrystal with selective adsorption for cationic dyes, Mater. Res. Bull., 83 (2016) 387–395.
[33] S. Yang, Y. Wu, A. Aierken, M. Zhang, P. Fang, Y. Fan, Z. Ming, Mono/competitive adsorption of Arsenic (III) and Nickel (II) using modified green tea waste, J. Taiwan Inst. Chem. Eng., 60 (2016) 213–221.
[34] O. Ajouyed, C. Hurel, M. Ammari, L.B. Allal, N. Marmier, Sorption of Cr (VI) onto natural iron and aluminum (oxy) hydroxides: effects of pH, ionic strength and initial concentration, J. Hazard. Mater., 174 (2010) 616–622.
[35] Y. Zhong, Q. Yang, K. Luo, X. Wu, X. Li, Y. Liu, W. Tang, G. Zeng, B. Peng, Fe(II)–Al(III) layered double hydroxides prepared by ultrasound-assisted co-precipitation method for the reduction of bromate, J. Hazard. Mater., 250 (2013) 345–353.
[36] V.K. Gupta, D. Pathania, S. Sharma, P. Singh, Preparation of bio-based porous carbon by microwave assisted phosphoric acid activation and its use for adsorption of Cr (VI), J. Colloid Interface Sci., 401 (2013) 125–132.
[37] M. Ghaedi, A. Ghaedi, B. Mirtamizdoust, S. Agarwal, V.K. Gupta, Simple and facile sonochemical synthesis of lead oxide nanoparticles loaded activated carbon and its application for methyl orange removal from aqueous phase, J. Mol. Liq., 213 (2016) 48–57.
[38] I. Langmuir, The adsorption of gases on plane surfaces of glass, mica and platinum, J. Am. Chem. Soc., 40 (1918) 1361–1403.
[39] H. Freundlich, Over the adsorption in solution, J. Phys. Chem., 57 (1906) e470.
[40] D. Bulgariu, L. Bulgariu, Equilibrium and kinetics studies of heavy metal ions biosorption on green algae waste biomass, Bioresour. Technol., 103 (2012) 489–493.
[41] H. Daraei, A. Mittal, M. Noorisepehr, J. Mittal, Separation of chromium from water samples using eggshell powder as a low-cost sorbent: kinetic and thermodynamic studies, Desal. Wat. Treat., 53 (2015) 214–220.
[42] A. Kara, E. Demirbel, N. Tekin, B. Osman, N. Beşirli, Magnetic vinylphenyl boronic acid microparticles for Cr (VI) adsorption: kinetic, isotherm and thermodynamic studies, J. Hazard. Mater., 286 (2015) 612–623.
[43] S.A.M. Idris, Adsorption, kinetic and thermodynamic studies for manganese extraction from aqueous medium using mesoporous silica, J. Colloid Interface Sci., 440 (2015) 84–90.
[44] L. Zhou, Y. Wang, Z. Liu, Q. Huang, Characteristics of equilibrium, kinetics studies for adsorption of Hg (II), Cu (II), and Ni (II) ions by thiourea-modified magnetic chitosan microspheres, J. Hazard. Mater., 161 (2009) 995–1002.
[45] C. Zhou, Q. Wu, T. Lei, I.I. Negulescu, Adsorption kinetic and equilibrium studies for methylene blue dye by partially hydrolyzed polyacrylamide/cellulose nanocrystal nanocomposite hydrogels, Chem. Eng. J., 251 (2014) 17–24.
[46] Z.A. Al-Othman, R. Ali, M. Naushad, Hexavalent chromium removal from aqueous medium by activated carbon prepared from peanut shell: adsorption kinetics, equilibrium and thermodynamic studies, Chem. Eng. J., 184 (2012) 238–247.
[47] Z.A. Al-Othman, M. Naushad, R. Ali, Kinetic, equilibrium isotherm and thermodynamic studies of Cr(VI) adsorption onto low-cost adsorbent developed from peanut shell activated with phosphoric acid, Environ. Sci. Pollut. Res., 20 (2013) 3351–3365.
[48] G. Sharma, M. Naushad, A.A.H. Al-Muhtaseb, A. Kumar, M.R. Khan, S. Kalia, Shweta, M. Bala, A. Sharma, Fabrication and characterization of chitosan-crosslinked-poly(alginic acid) nanohydrogel for adsorptive removal of Cr(VI) metal ion from aqueous medium, Int. J. Biol. Macromol., 95 (2017) 484–493.
[49] S. Yang, Y. Wu, A. Aierken, M. Zhang, P. Fang, Y. Fan, Z. Ming, Mono/competitive adsorption of Arsenic(III) and Nickel(II) using modified green tea waste, J. Taiwan Inst. Chem. Eng., 60 (2016) 213–221.
[50] T. Sumathi, G. Alagumuthu, Adsorption studies for arsenic removal using activated *Moringa oleifera*, Int. J. Chem. Eng., 2014 (2014) 1–6.
[51] P. Gore, M. Khraisheh, B. Kandasubramanian, Nanofibers of resorcinol–formaldehyde for effective adsorption of As (III) ions from mimicked effluents, Environ. Sci. Pollut. Res., 25 (2018) 1–17.
[52] S. Allen, G. Mckay, J. Porter, Adsorption isotherm models for basic dye adsorption by peat in single and binary component systems, J. Colloid Interface Sci., 280 (2004) 322–333.
[53] E. Sibbesen, Some new equations to describe phosphate sorption by soils, J. Soil Sci., 32 (1981) 67–74.
[54] Y. Yan, Q. An, Z. Xiao, W. Zheng, S. Zhai, Flexible core-shell/bead-like alginate@PEI with exceptional adsorption capacity, recycling performance toward batch and column sorption of Cr(VI), Chem. Eng. J., 313 (2017) 475–486.

Supplementary information:

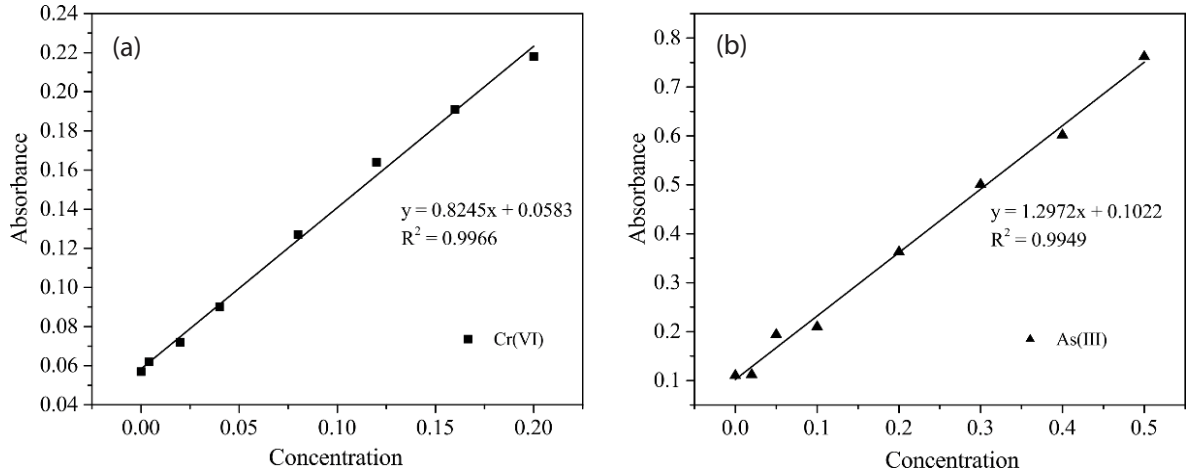

Fig. S1. The calibration curves for measuring Cr(VI) (a) and As(III) (b) concentrations.

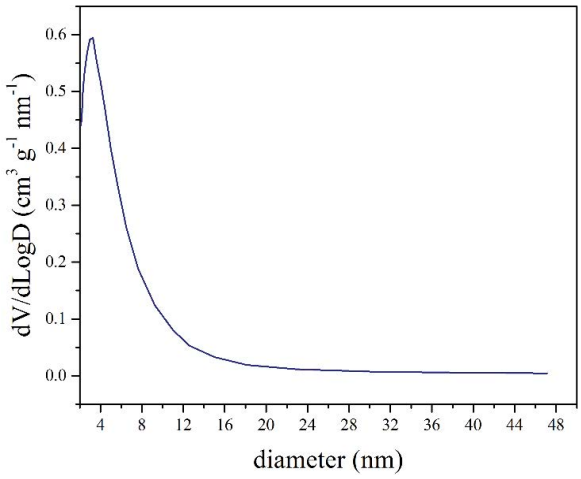

Fig. S2. The pore size distribution of original Fe-Al hydroxides.

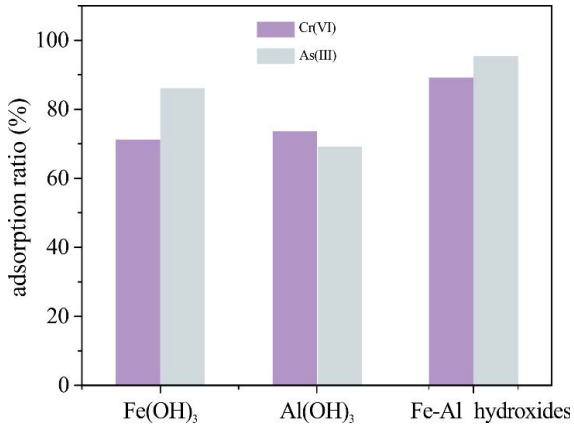

Fig. S3. The adsorption capability of Cr(VI) and As(III) by pure $Fe(OH)_3$, pure $Al(OH)_3$, and Fe-Al hydroxides.

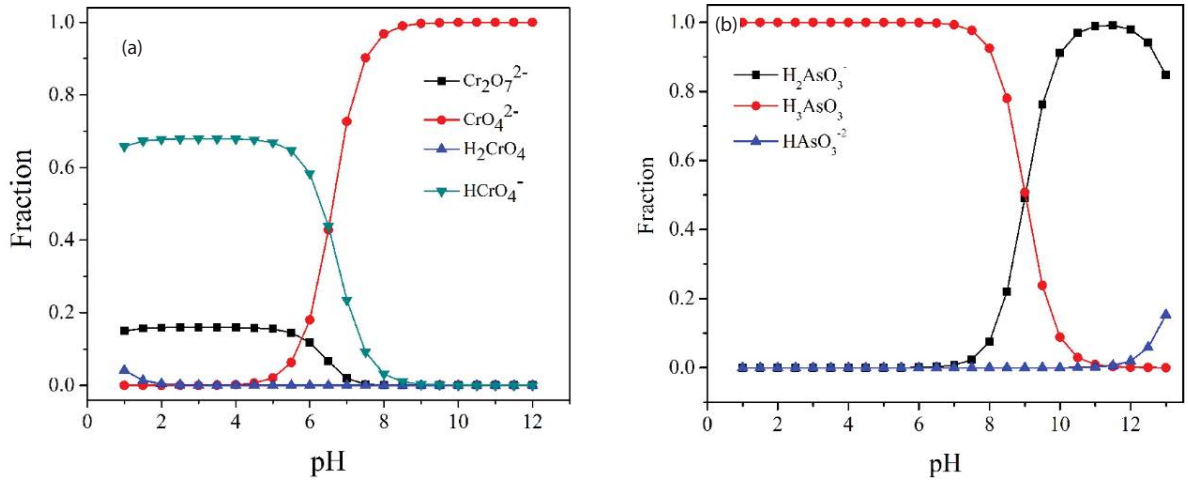

Fig. S4. Diagram for Cr(VI) (a) and As(III) (b) chemical species in aqueous solution.

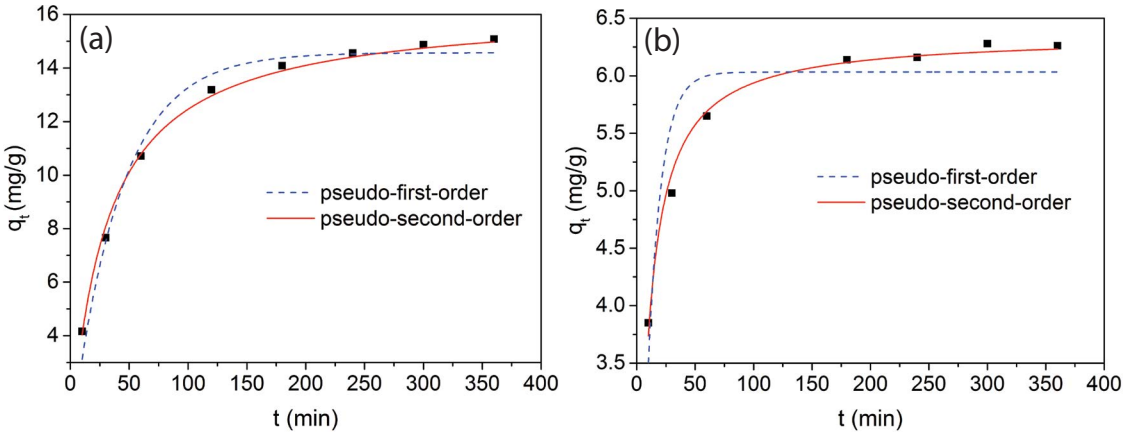

Fig. S5. The kinetic model for adsorption of Cr(VI) (a) and As(III) (b).

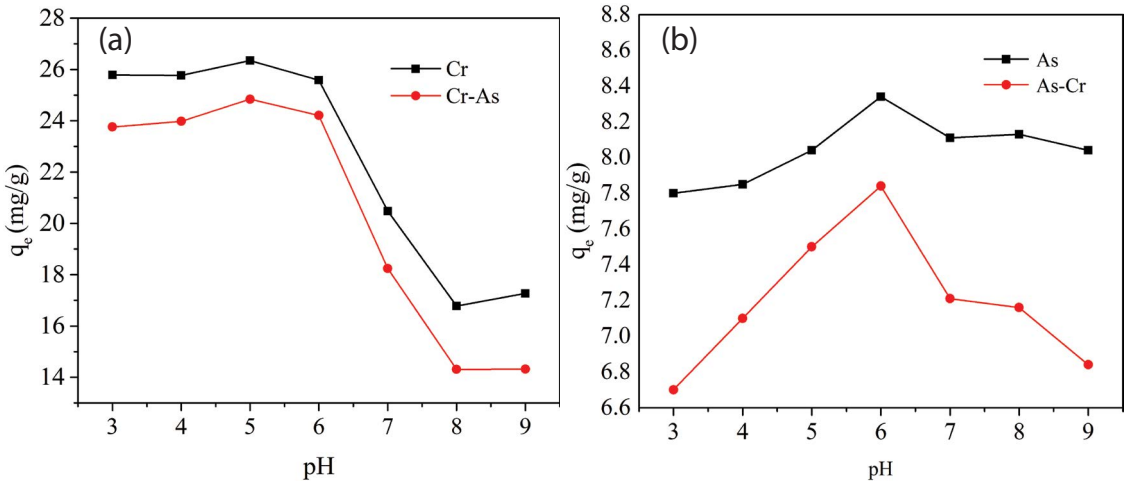

Fig. S6. Effect of pH on the adsorption of (a) Cr(VI) and (b) As(III) in binary component system.

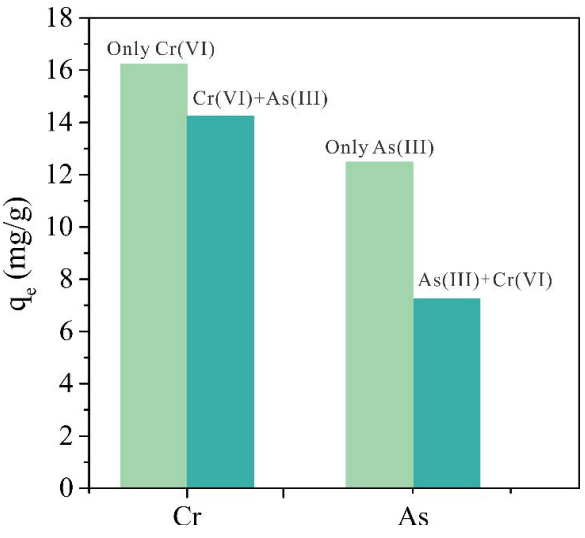

Fig. S7. The comparison of adsorption capacity for Cr(VI) and As(III) in single and binary system. The concentration for each heavy metal is 0.5 mM.

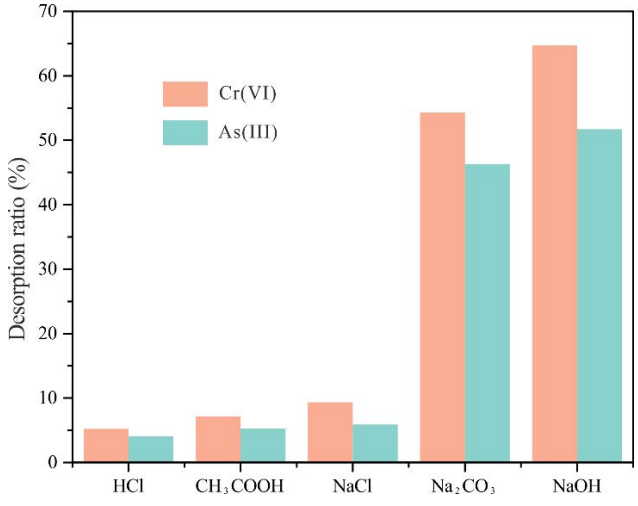

Fig. S8. The desorption performance of Fe-Al hydroxides with different eluents.

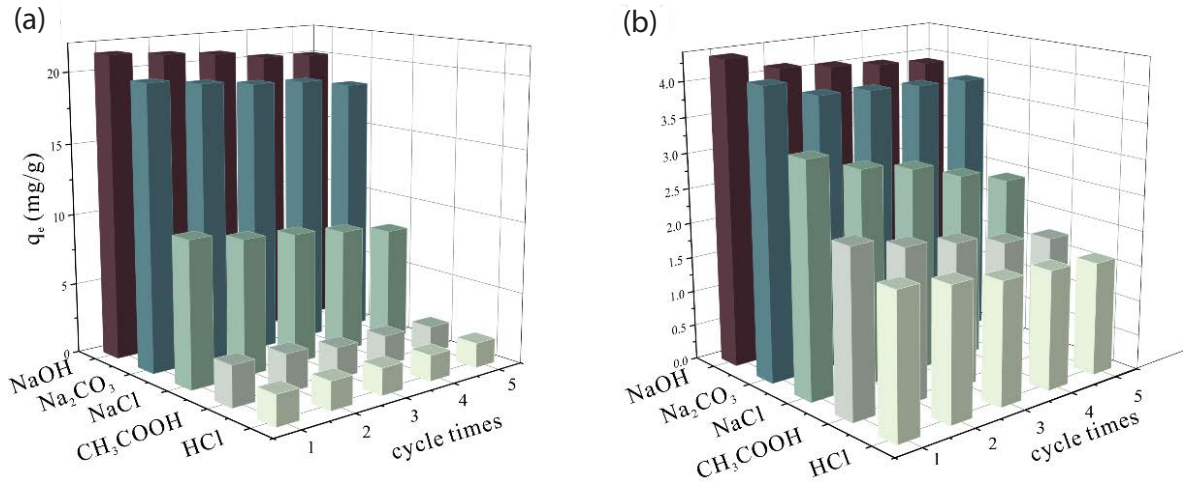

Fig. S9. The reusability of Fe-Al hydroxides for Cr(VI) (a) and As(III) (b) after different cycle times with different eluents.